STRENGTH AND STABILITY OF TRADITIONAL TIMBER FRAMES

André Jorissen[1], Jordan Dorlijn[2], Ad Leijten[3] and Bert Snijder[4]

ABSTRACT: This paper reports the on-going research into traditional timber frames at the Eindhoven University of Technology (TU/e) in the Netherlands, see e.g. [1] for a paper presented at WCTE 2014. Traditional timber frames were common structures for centuries. They lost popularity due to high manufacturing costs and low rated perception related to durability and load carrying capacity. Today's technology provides timber frames and especially connections with high precision at relatively low production costs. This, together with the fact that these structures are still appealing, result in an increasing popularity although, as shown in this paper, the load carrying capacity of the frame regarded as a sway system is (very) low. The realisation of traditional timber frames is still based on craftsmanship without knowledge about strength, stability and stiffness. Traditional portal frames as shown in figure 1 are analysed. The analyses of numerical and experimental results show the peg diameter to be decisive for the mortise and tenon stiffness for which a design formula is derived.

KEYWORDS: Traditional timber frames, mortise and tenon connections

1 INTRODUCTION

Traditional portal frames as shown in figure 1 are analysed.
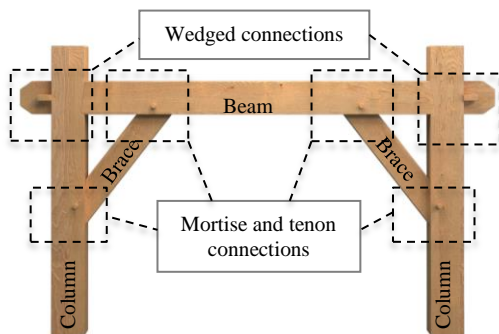
Figure 1: Timber frames studied (figure based on [2])

To increase the knowledge about the behaviour of traditional timber frames, experimental, analytical and numerical research is carried out. The experiments are reported in [1] and [5]. Further analytical and numerical research is reported in this paper and in [6]. From this analysis design rules can be derived for both the load carrying capacity (first and second order) and stiffness of the frame. Many experiments on mortise and tenon connections have been reported in e.g. [3], on which accurate capacity design rules for these connections are derived. However, little research is reported on the stiffness of these connections and on the behaviour of the whole structure.

The objective of the research described in the paper is to develop design rules for strength (stability) and stiffness of traditional portal frames weakened by the mortise and tenon connections.

The connections studied are shown in figure (2)
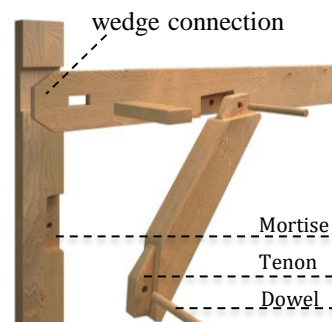
Figure 2: Connections studied (figure based on [2])

This type of construction is frequently applied over the centuries in relatively large constructions. After the Second World War, the application almost disappeared due to the required (missing) craftsmanship and high costs (manual labour). The constructions are made

---

[1] André Jorissen, Eindhoven University of Technology (TU/e), Den Dolech 2, 5612 AZ Eindhoven and SHR Timber Research, Nieuwe Kanaal 9b, 6709 PA, Wageningen, The Netherlands. E-mail: a.j.m.jorissen@tue.nl

[2] Jordan Dorlijn, Eindhoven University of Technology (TU/e) Den Dolech 2, 5612 AZ Eindhoven. E-mail dorlijnj@gmail.com

[3] Ad Leijten, Eindhoven University of Technology (TU/e), Den Dolech 2, 5612 AZ Eindhoven, The Netherlands. E-mail: a.j.m.leijten@tue.nl

[4] Bert Snijder, Eindhoven University of Technology (TU/e), Den Dolech 2, 5612 AZ Eindhoven. E-mail: h.h.snijder@tue.nl

regularly again today; effective industrial processes reduce the costs and demands on the craftsmanship.

As the popularity rises more understanding of the behaviour is required in order to continue to ensure safety. The design of the structure is still mostly based on experience without knowledge of the actual strength, stability and rigidity.

The research described in this paper indicates, that, considering the fact that the mechanical behaviour, also on the side where the brace is in compression, is determined by the dowel, the relatively flexible mortise-tenon connections reduces the load carrying capacity up to 80%. The flexible mortise-tenon connections also increases the so-called second order movements compared to the situation without these flexible connections. This reduces the critical load, defined as the axial load carrying capacity by the frame columns, in case of a combination of horizontal and vertical loads, considerably compared to the situation without the flexibility of the joints.

It is therefore highly important to investigate the stiffness of the connections and study the effect on the strength, rigidity and stability of the frame.

2 ANALYTICAL ANALYSES

2.1 MORTISE AND TENON CONNECTION STRENGTH AND STIFFNESS

Strength models for the mortise and tenon connections reported in literature regarded are based on the original so-called Johansen [4] equations, for which elastic properties of the fastener are used (and not elastic-plastic properties as for the later developed European Yield Model[10]) and therefore suitable for wooden dowel type fasteners. Consequently, brittle failure modes are assumed not to be determining.

Equations (1) to (5) show the load carrying capacity per dowel according to the Johansen principle; the corresponding failure modes are shown in figure 3 [3].

Mode I:
$$F_{Im} = dt_m f_{em} \tag{1}$$

Mode II:
$$F_{Im} = 2dt_s f_{es} \tag{2}$$

Mode III:
$$F_{III} = \frac{2dt_s f_{em} f_{es}}{2f_{es} + f_{em}}\left(\sqrt{Q} - 1\right) \tag{3}$$

$$Q = \frac{2(f_{es} + f_{em})}{f_{em}} + \frac{2f_{yb}(2f_{es} + f_{em})d^2}{3f_{em}f_{es}t_s^2}$$

Mode IV:
$$F_{IV} = 2d^2\left(\frac{2f_{yb}f_{em}f_{es}}{3(f_{es} + f_{em})}\right) \tag{4}$$

Mode V:
$$F_V = \frac{1}{2}\pi d^2 f_{ev} \tag{5}$$

With

F_i	Connection strength according to mode i	[N]
d	Dowel diameter	[mm]
t_s	Side member thickness (beam/column)	[mm]
t_m	Middle member thickness (tenon)	[mm]
f_{em}	Tenon embedment strength	[N/mm^2]
f_{es}	Side member embedment strength	[N/mm^2]
f_{ev}	Fastener shear strength	[N/mm^2]
f_{yb}	Fastener bending strength	[N/mm^2]
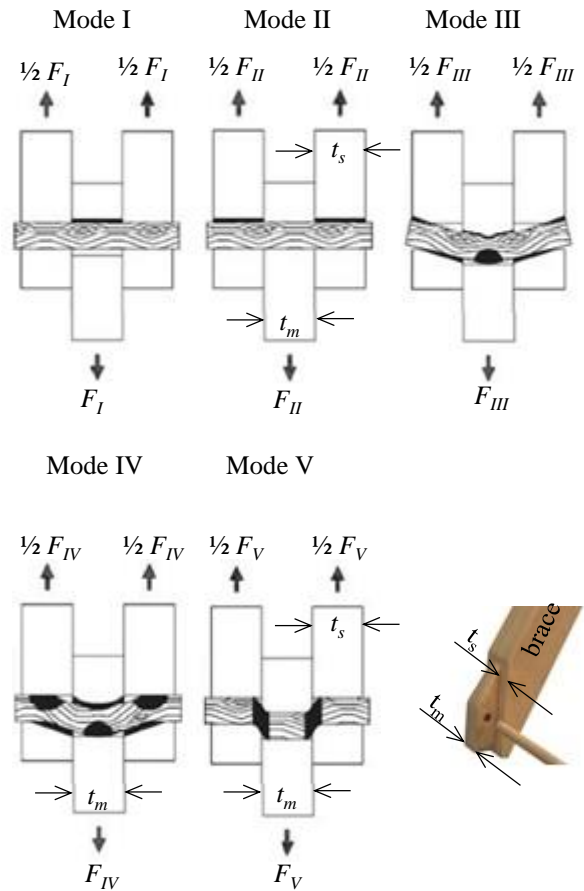
Figure 3: Failure mechanism [3]

For the stiffness of these connections a spring model, already described in [1] and [5], is used. Since the stiffness is defined in the elastic state, different contributions can be superposed. The connection deformation is due to (first) the embedment in the pen (tenon), (second) the dowel deformation and (third) the embedment in the column/beam ("support"). The superposition of these contributions is illustrated in figure 4.

$$\Delta = \frac{F}{k_{tenon}} + \frac{F}{k_{dowel}} + \frac{F}{2 k_{\text{"sup port"}}} = \frac{F}{k_c}$$

$$k_c = \frac{2 k_{tenon} k_{dowel} k_{\text{"sup port"}}}{k_{tenon} + k_{dowel} + 2 k_{\text{sup port}}} \qquad (6)$$
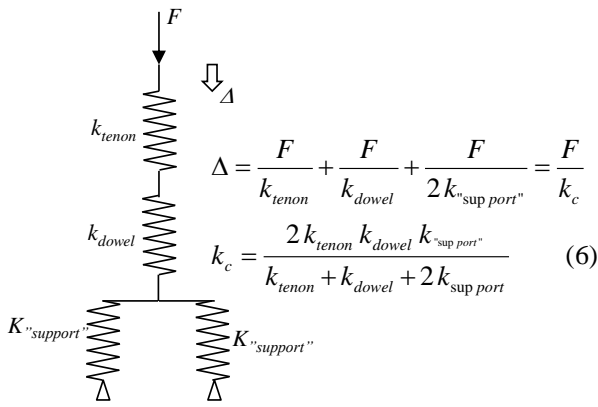
Figure 4: Mortise-tenon connection stiffness modelling [5]

2.2 FRAME BEHAVIOUR

The frame considered is shown in figure 5. The connections are schematized by translational springs with spring stiffness '$k_{\theta B}$' for the beam side connections and '$k_{\theta C}$' for the column side connections.

The structure is loaded with a horizontal point load F_H and vertical point loads F_V. Brace angles are represented by 'θ_C' and 'θ_B' (respectively column-brace and beam-brace angles).
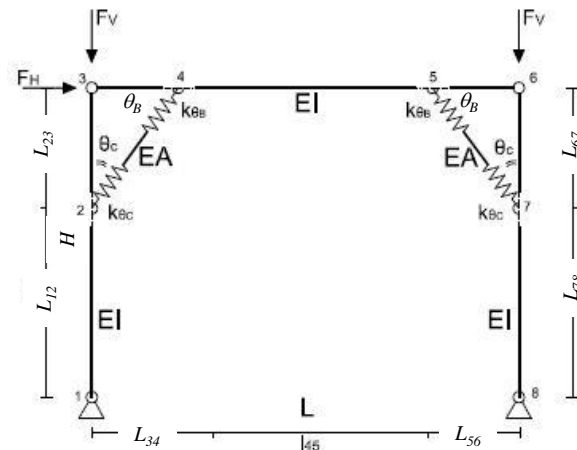
Figure 5: Mechanical model of the frame

The frame is regarded as a so-called sway – frame of which the displacements are indicated in figure 6.
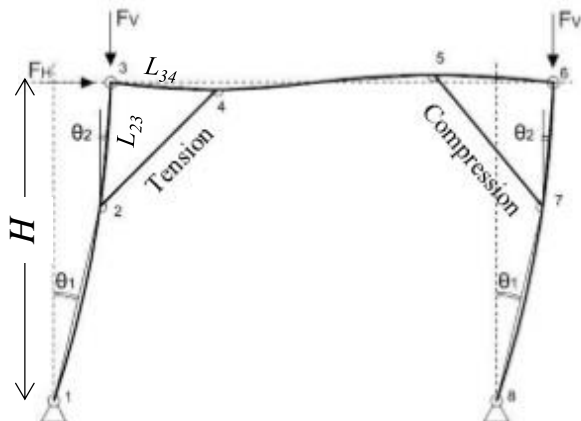
Figure 6: Sway movement of the frame

Distinction can be made between tension side behaviour and compression side behaviour although the behaviour is similar up to a certain extend. The behaviour is completely different when in the compression brace member contact is made with the beam / column and the load is transferred by bearing. However, shrinkage of the connection causes gaps up to 3-4 mm which causes the connections both in tension and compression behave similar (the brace force is transferred by the dowel both in tension and compression).

The wedge connection (see figures 1 and 2), can be regarded as a hinge (for realistic brace lengths this connection hardly contributes to the stiffness). For the strength and stability of the frames, the stiffness of the braces, and especially the stiffness of the mortise-tenon connections, is determining; actually the stiffness of the triangle realised by the brace, column and beam, as indicated in figure 7. For the analytical stability analyses of the frame Dunkerley's theorem [7] is used to find the total buckling load F_c, of which the principle is shown in figure 7 and equation (7).
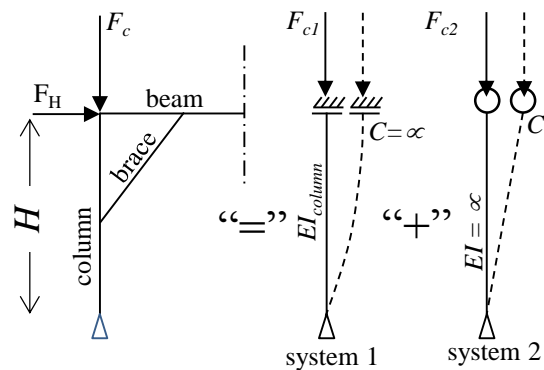
C = stiffness provided by the triangle
brace – column - beam

Figure 7:Dunkerley's theorem [7]

$$\frac{1}{F_c} = \frac{1}{F_{c1}} + \frac{1}{F_{c2}} \qquad (7)$$

For both F_{c1} and F_{c2} equations are analytically derived and consequently the critical load F_c can be determined. For system 1 it is assumed, that the brace, including the connections to the beam and column, is infinitely stiff while the beam and column have their original stiffness. For system 2 it is the opposite: the brace, including the connections to beam and column, have their original stiffness while the beam and column are regarded with an infinite stiffness. Thus, in principle the systems as shown in figure 8 are analysed.

The analytical result of system 1 is not an equation suitable for hand calculation. However, the load carrying capacity of system 1 is so high compared to that of system 2, as indicated in figure 14, that in fact only system 2 has to be considered. The result for system 2,

being a very good approximation for the complete timber frame, is given by equation (8).

$$F_c = F_{c2} = k_{brace} \frac{L_{23}^2 \cdot L_{34}^2}{H\left(L_{23}^2 + L_{34}^2\right)} \ [N] \qquad (8)$$

With k_{brace} [N/mm]   see figure 8
            L_{23} and L_{34} [mm]   see figure 5
            H [mm]   see figure 5 and 7
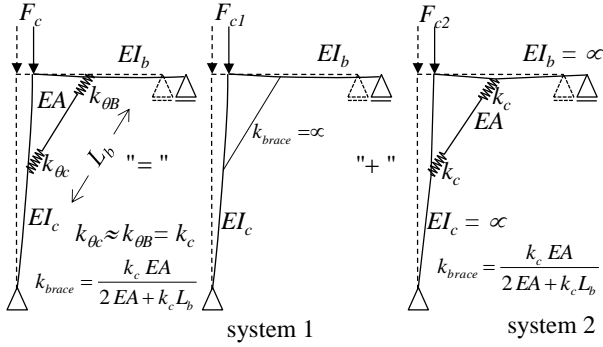
Figure 8: Buckling systems

Furthermore, First and second order deflections are analysed. Taking k_{brace} as defined in figure 8 into account first order deflections (w_{1st}) can be derived. The second order deflections (w_{2nd}) are determined with equation (9).

$$w_{2nd} = w_{1st} \frac{n}{n-1} [mm] \qquad (9)$$

In which $n = \dfrac{F_c}{F_{applied}}$

An equilibrium analyses in the deformed situation, taking the second order displacement w_{2nd} into account, results in forces and bending moments in the timber frame elements of which usually the tension force in one of the braces is determining.

3 NUMERICAL ANALYSES

The numerical analyses focuses on the mortise and tenon connection behaviour and on stability (second order – equilibrium in the deformed situation).

3.1 MORTISE AND TENON CONNECTION STIFFNESS

Firstly, a finite element model of the mortise and tenon connections was built in Abacus version 6.13.1 with a number of changeable parameters: grain angle "α", dowel diameter "d", tenon width "t_m" and beam and column width "b" ($b = 2t_s + t_m$ as shown in figure 9).
In order to reduce calculation time, a quarter of the connection is modelled, which is possible due to double symmetry of the connection. The following boundary conditions are applied:

plane 1 (front): $ru_z = 0$, $ru_y = 0$, $u_x = 0$;
plane 2 (right side): $ru_x = 0$, $ru_y = 0$, $u_z = 0$;

plane 3 (grey area): $u_x = 0$, $u_y = 0$, $u_z = 0$.

u_i = displacement in 'i' direction
ru_i = rotation around 'i'-axis

Remark: plane indications are given in figure 9.
R.P. is the point of reference considering displacements
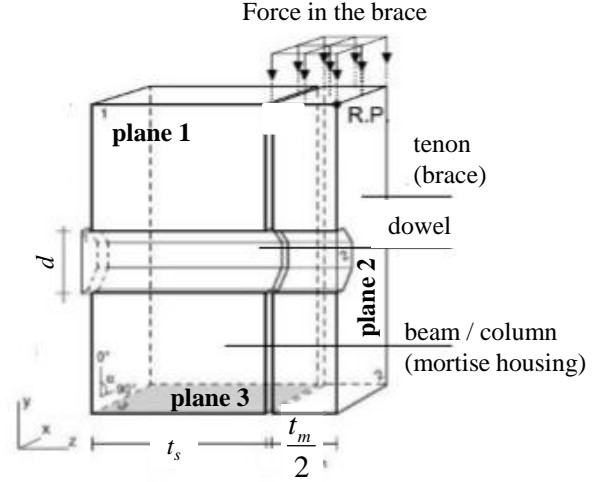
Figure 9: Numerical model of the connection

The connection is modelled with 8-node (linear) elements. A (quasi-) isotropic material model is used for the main and side members, because the members are mainly loaded in one direction. Material properties in an angle to the grain are obtained by using a Hankinson interpolation between parallel (f_0) and perpendicular (f_{90}) material properties for both strength and stiffness. according to equation (10), based on [8].

$$f_\alpha = \frac{f_0 \, f_{90}}{f_0 \sin^2(\alpha) + f_{90} \cos^2(\alpha)} \qquad (10)$$

In which   strength $f_0 = 26$ N/mm^2
                     $f_{90} = 5,0$ N/mm^2
         stiffness $E_0 = 11540$ N/mm^2
                     $E_{90} = 350$ N/mm^2

The dowel is given an orthotropic material model, due to loading in multiple directions, of which the stiffness matrix '[D]' is given in [6], based on experiments on "dry" European Oak (average moisture content of 20%) described in [5].
Poisson ratios are taken as: $\mu_{XY} = \mu_{XZ} = \mu_{YZ} = \mu_{ZY} = 0,41$ and $\mu_{YX} = \mu_{ZX} = 0,061$; these values are based on [11].

The numerical model is verified with experimental data from [5], actually an embedment test resulting in a load-slip curve from which the stiffness is determined, which are shown in table (1).

Table 1: *Experimental connection stiffness [5]*

$K_{\theta C}=K_{\theta B}$ [N/mm]	$\theta = \alpha = 38^o$	$\theta = \alpha = 52^o$
Specimen 1	5534	5268
Specimen 2	4770	6097
Specimen 3	6450	-
Average	5585	5683

Experimental tests were performed on connections with a width of $b = 150$ mm, dowel diameter '$d = 22$ mm', tenon width of $t_m = 37,5$ mm (a quarter of the connection width) and side member width '$t_s = 56,25$ mm' ($^3/_8$ of the connection width) , see figure (10).
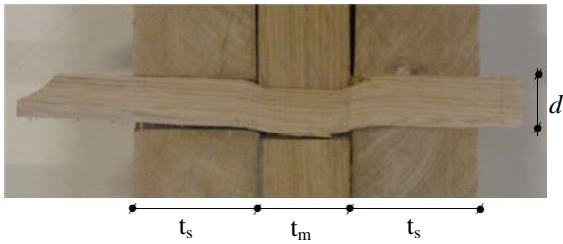
Figure 10: *Cutting of experimental test, from [5]*

As mentioned in table 1, two grain angles have been tested, namely 38° and 52°. Table 2 shows the numerical results for these grain angles.

Table 2: *Numerical connection stiffness K_C [6]*

	$\theta = \alpha = 38^o$	$\theta = \alpha = 52^o$
Num. stiffness *[N/mm]*	6900	6320

Surprisingly, experimental results show a slight increase in stiffness for a grain angle of 52° (closer to perpendicular to the grain). The high spread in experimental results shows the connection's sensitivity to imperfections. Furthermore, although the stiffness values according to the numerical model are higher compared to the experimental values (up to approximately 20%, which is approximately equal to the spread in the experimental results), the numerical results are used for further frame analysis.

The numerical analysis is based on the set of geometrical parameters given in table 3. The tenon width t_m is taken as a quarter of the connection width; since loads are mainly transferred by shear in the dowel the tenon width hardly influences the connection stiffness.

Table 3: *Parameter set*

Beam width	Dowel (peg) diameter	Grain angle
125 mm	18 mm	
150 mm	20 mm	30°
200 mm	22 mm	45^0
300 mm	27 mm	60^0
400 mm	38 mm	

Remark: thus 75 different set-ups are analysed.

The grain angle follows from the angle of the brace with the column and beam, figure 5. Common brace angles vary between 30° and 60^0.

The results for a beam width of 125 mm and 400 mm are shown in respectively figure 11 and 12. Other beam widths give the same type of result (proportional to the peg diameter *d*) and are therefore not elaborated in this paper. Full results can be found in [6].

Each figure shows three trend lines representing the three grain angles 'a30-a45-a60' numerically evaluated. The points in the graph represent the connection stiffness for the chosen peg diameters (table 3).
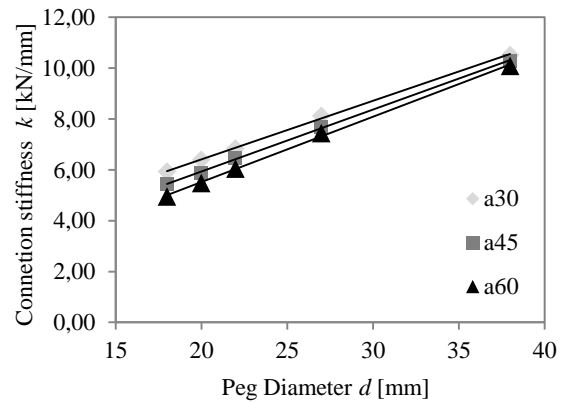
Figure 11: *Results for 125 mm beam / column width*
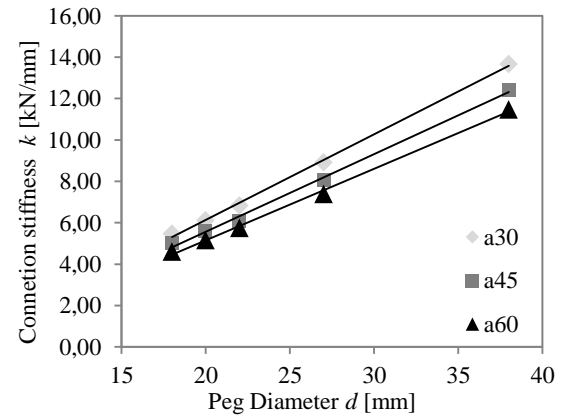
Figure 12: *Results for 400 mm beam/ column width*

The results show a clear linear relation between peg diameter and connections stiffness for all results. In order to analyse the influence of the beam width on the connection stiffness, the slopes of the trend lines for all beam widths, are plotted, figure (13).
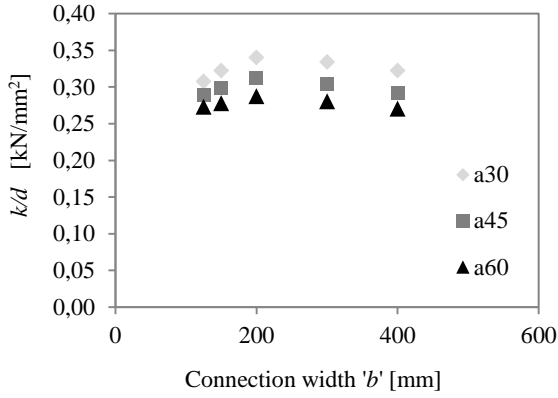
Figure 13: Relative stiffness k/d

The highest connection stiffness is found at a connection width of 200 mm for all three grain angles.

The difference in connection stiffness between the maximum found stiffness at b = 200 mm and the minimum at b = 125 mm, is less than 10 %, which is less than the spread in experimental results. Therefore the influence of connection width on the connection stiffness is neglected, so that the connection stiffness can be described by equation shown (11).

$$k_{\theta C} = k_{\theta B} = k_c = A \cdot d \qquad (11)$$

In which: $k_{\theta C} = k_{\theta B} = k_c$= the connection stiffness in
  [kN/mm] as indicated in figure 8.
  A material factor depending on the
     material properties and grain angle in
     [kN/mm^2],
  d the peg diameter in [mm].

The material factors 'A', for this particular research based on European dry oak, are given in table (4) for the three investigated grain angles.

Table 4: Material factors 'A' [kN/mm^2]

	$\alpha = 30^{\circ}$	$\alpha = 45^{\circ}$	$\alpha = 60^{\circ}$
A	0,32	0,30	0,28

3.2 TIMBER FRAME ANALYSIS

The timber frame analysed is shown in figure 5. First buckling is considered numerically. After, full structural behaviour is analysed including buckling, first and second order deflections and failure in which both horizontal and vertical loading, as indicated in figure 5, are considered. Based on these analysis design rules are extracted that estimate horizontal and vertical load capacity.

The frame is simulated in Abaqus 6.13.1 with 'B21' 2 node linear elements and analysed for system 1, system 2 and the total system in order to find the influence of connection stiffness on the buckling load.

Figure 14 shows the result for a number of frames considered. Not only the numerical results are plotted; also the analytical results according to the analytical analysis discussed related to figure 7 are plotted. The analytical results for system 2 can be verified using equation (8). The following geometrical parameters (see figure 5) are used:

- Frame height H = 2500 mm
  Frame length L = 5000 mm
  $L_{23} = L_{34}$ = 1000 mm
  θ = 45^0 for both the beam and column connection
- One dowel at both the column and beam to brace connection.
- Timber element cross section:
  Beam / column: b = 300 mm
           h = 300 mm
  Brace: b = 125 mm
           h = 250 mm
- Material: European Oak – moisture content $\omega \approx$ 20%
  E = 11500 N/mm^2
- Peg (dowel) diameter d = 27 mm
- k_{brace} = 4 kN/mm (figure 8)

Figure 14 shows the buckling load for both systems 1 and 2 (see figure 7) and the total (combined) system. For both the numerical and analytical approaches these systems are analysed separately after which the analytical results are combined using equation (7). The y-axis represents the buckling load in [kN], the x-axis the brace distance in [mm] (L_{23}, L_{34}, L_{56} and L_{67} in figure 5). A brace distance of 2500 mm shows non-sway buckling as a trussed type frame is formed.

For all systems analytical (striped lines) and numerical results (dots) are plotted. Because the analytical en numerical results for system 2 and also for the combined results are almost identical, there is no clear visible difference between the results.
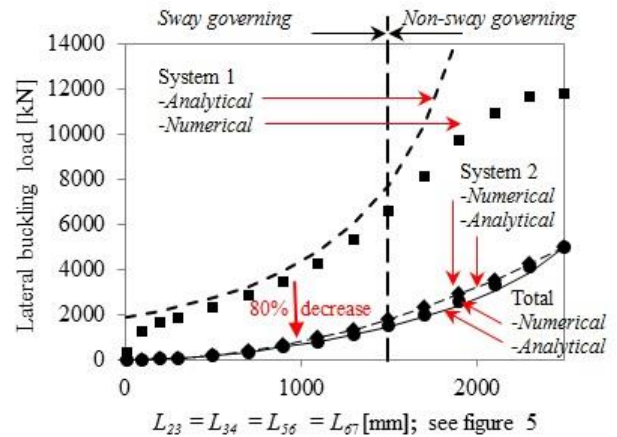
Figure 14: Buckling results

The analytical results of system 1 compared to the numerical, differentiate for $L_{34} = L_{56} > 1500$ mm brace distance. This is due to the assumption during the analytical analysis that sway is governing, while non-sway buckling becomes governing when brace distances become larger. Therefore the analytical results for sway-type buckling become infinite.

Itis clear that the results of system 2 are close to the results of the combined (or total) system. This indicates that buckling due to the low connection stiffness (system 2) governs the system. For a practical brace distance of 1000 mm, an 80% decrease in buckling compared to system 1 load is found Thus, when a sway system is expected to be the governing system, the connection system has to be taken into account.

In that case, system 2 overestimates the total buckling load with less than 10% and is therefore a good approximation.

As discussed earlier, second order deformations are determined by equation (9) with the applied force, the buckling load and first order deflections w_{1st}, indicated in figure 15.
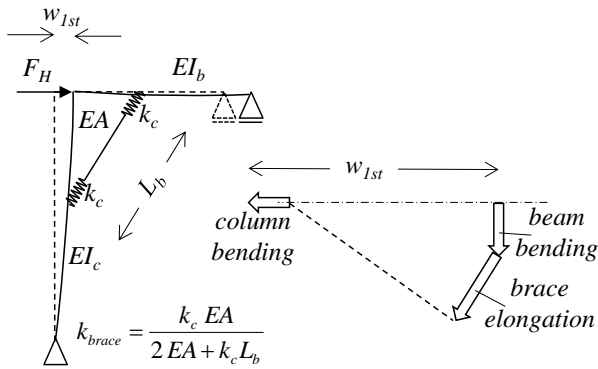
Figure 15: *First order frame displacements w_{1st}.*

The horizontal load capacity is determined by first order forces and the capacity of the connection, as they are the weakest link. The structure can still hold some force after failure of connections in tension, as it is still supported by the compression side. However, after connection failure, the compression side carries the full bending moment of the frame for which, in some configurations, it doesn't hold enough strength. Therefore failure of a connection in tension is considered as frame failure.

First order frame failure (due to a horizontal point load $F_{u,H}$) is determined by equilibrium and given by equation (12).

$$F_{u,H,1st} = \frac{2F_{u;connection}\sin\theta_c l_{23}}{H} \quad (12)$$

With:

$F_{u,H,1st}$	Horizontal load capacity	[N]
$F_{u;connection}$	Connection strength	[N]

For second order frame failure analyses the frame deformations, determined according to equation (9), have to be taken into account (due to second order moments, less horizontal force can be applied. Equilibrium analyses of the deformed structure results in the horizontal load carrying capacity $F_{u,H.2nd}$ when the frame is also loaded with a vertical force $F_{u,V}$ according to equation (13).

$$F_{u;H,2nd} = \frac{2\left(F_{u;connection}\sin\theta_c L_{23} - F_{u;V}w_{2nd}\right)}{H} \quad (13)$$

With:

$F_{u,H,2st}$	Horizontal load capacity	[N]
w_{nd}	Second order displacement determined according to equation (9) [mm]	
$F_{u,V}$	Applied vertical load	[N]

Rewritten the other way around, the result is the vertical load carrying capacity $F_{u,V,nd}$ when the frame is also loaded with a given horizontal load $F_{u,H}$; the result is equation (14).

$$F_{u;V,2nd} = \frac{F_{u;connection}\sin\theta_c L_{23} - \frac{1}{2}F_{u;H}H}{w_{2nd}} \quad (14)$$

$F_{u,V,2st}$	Vertical load capacity	[N]
$F_{u,H}$	Applied horizontal load	[N]

Based on equation (13) or (14) an interaction diagram can be made between horizontal and vertical loads applied in combination with the dowel diameter, as the capacity and stiffness of the structure is determined by the mortise and tenon connections. Figure 16 shows this interaction diagram for the frame example for which the geometrical parameters are given in 3.2. Second order displacements are determined by (9). The mortise and tenon brace-column and brace-beam connections both hold 2 pegs. The brace stiffness therefore

$$K_{brace} = \frac{2k_cEA}{2EA + 2k_cL_b} = \frac{k_cEA}{EA + k_cL_b} \text{ [kN/mm].}$$
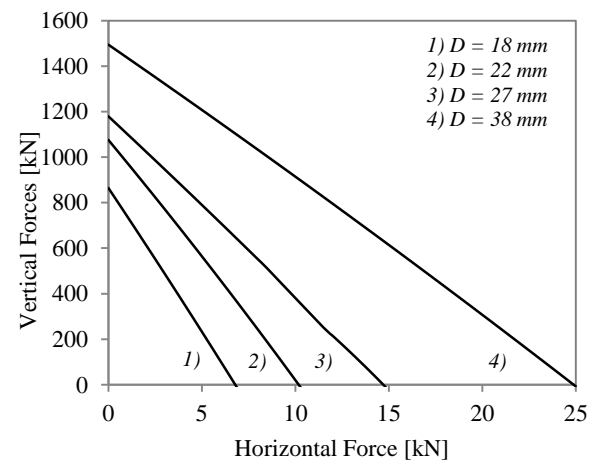
Figure 15: *Load interaction diagram*

The interaction diagram clearly shows the influence of the dowel diameter on the horizontal and vertical load capacity of the structure. When zero horizontal load is applied, the graph gives the critical load F_c, equation (8), and when zero vertical load is applied the maximum first

order horizontal load according to equation (12) is found.

4 EXPERIMENTAL TESTS

No tests on full seize traditional timber portal frames are carried out at TU/e up to now. The experimental research referred to is the research carried out described in [1] and [5].

5 CONCLUSIONS

From the experiments and the numerical simulations it is clear that the peg diameter is the most determining parameter for mortise and tenon stiffness, for the brace stiffness and for the total frame stiffness.
It is even possible to derive a simple equation like equation (11).

Consequently, the stiffness of the brace, and the load carrying capacity F_c can be increased by increasing the wooden dowel diameter. It must be said that the results for the material factor 'A' presented in this paper (table 4) only account for dry European Oak with a moisture content of 20% average. For other wood species and moisture contents, this factor is possibly different.

The load carrying capacity F_c of a traditional timber portal frame determined with a second order analyses in Abaqus, equals to the analytically determined load carrying capacity according to equation (8).

Maximum load carrying capacity of the frame is determined by the strength of the mortise and tenon connections, ($F_{u;connection}$) and the interaction between horizontal F_H, and vertical $\underline{F}_V$, point loads; the relationship between these parameters are given by equation (14).

REFERENCES
[1] André Jorissen, Jaco den Hamer, Ad Leijten. Traditional Timber Frames. In: *Proceedings of WCTE 2014*, Quebec City, Canada, 2014.
[2] D. Venmans. Vidi Visuals. http://www.vidivisuals.com. 2014.
[3] R.J. Schmidt, R.B. MacKayand B.L. Leu. Design of joints in Traditional Timber Frame Buildings. In: *Proceedings of WCTE 1996*, New Orleans, USA, 1996.
[4] K.W. Johansen. Theory of timber connections. *International Association of Bridge and Structural Engineering*. Publication 9, Basel, Switzerland, 1949.
[5] J.C. den Hamer. Experimental research of the traditional wooden braced frame. *Master Thesis. Eindhoven University of Technology*, The Netherlands, 2014.
[6] Jordan Dorlijn. A research towards design rules for the strength and stability of traditional timber portal frames with mortise and tenon bracing. *Master Thesis. Eindhoven University of Technology*, The Netherlands, 2015.
[7] S. Dunkerley. On the whirling and vibration of shafts. *Phil. Trans. Roy. Soc*. London, 1894.
[8] R. L. Hankinson. "Investigation of crushing strength of spruce at varying angles to the grain," *Air Serv. Inf. Circ.*, vol. 3, no. 259 (material section paper No. 130), 1921.
[9] Merchant, W. The failure load of rigidly jointed framework as influenced by stability. *Structural Engineering,* volume 32, p. 185, London 1954
[10] Adolf Meyer. Die Tragfähigkeit von Nagelverbindungen bei statischer Belastung. *Holz als Roh- und Werkstoff*, 15 Jg. Heft 2, S. 96-109, 1957.
[11] Dietenberger M.A., Green D. Wood Handbook, wood as an engineering material. *USDA Forest Service*, Madision, Wisconsin, 1999.